Title

Codeposition Enhances the Performance of Electrochemical Aptamer-Based Sensors.

Journal

Langmuir, 40(16)

Authors

Wu, Yuyang

Shi, Jinyuan

Kippin, Tod

et al.

Publication Date

2024-04-23

DOI

10.1021/acs.langmuir.4c00585

Peer reviewed

HHS Public Access

Author manuscript

Langmuir. Author manuscript; available in PMC 2025 February 13.

Published in final edited form as:

Langmuir. 2024 April 23; 40(16): 8703–8710. doi:10.1021/acs.langmuir.4c00585.

Codeposition Enhances the Performance of Electrochemical Aptamer-Based Sensors

Yuyang Wu,
Department of Chemistry and Biochemistry, University of California Santa Barbara, Santa Barbara, California 93106, United States

Jinyuan Shi,
Department of Chemistry and Biochemistry, University of California Santa Barbara, Santa Barbara, California 93106, United States

Tod E. Kippin,
Department of Psychological and Brain Sciences and Biological Engineering Graduate Program, University of California Santa Barbara, Santa Barbara, California 93106, United States; Department of Molecular Cellular and Developmental Biology and Neuroscience Research Institute, University of California, Santa Barbara, California 93106, United States

Kevin W. Plaxco
Department of Chemistry and Biochemistry and Biological Engineering Graduate Program, University of California Santa Barbara, Santa Barbara, California 93106, United States

Abstract

Electrochemical aptamer-based (EAB) sensors, a minimally invasive means of performing high-frequency, real-time measurement of drugs and biomarkers in situ in the body, have traditionally been fabricated by depositing their target-recognizing aptamer onto an interrogating gold electrode using a “sequential” two-step method involving deposition of the thiol-modified oligonucleotide (typically for 1 h) followed by incubation in mercaptohexanol solution (typically overnight) to complete the formation of a stable, self-assembled monolayer. Here we use EAB sensors targeting vancomycin, tryptophan, and phenylalanine to show that “codeposition”, a less commonly employed EAB fabrication method in which the thiol-modified aptamer and the mercaptohexanol diluent are deposited on the electrode simultaneously and for as little as 1 h, improves the signal

Corresponding Author: **Kevin W. Plaxco** – Department of Chemistry and Biochemistry and Biological Engineering Graduate Program, University of California Santa Barbara, Santa Barbara, California 93106, United States; kwp@ucsb.edu.

Supporting Information

The Supporting Information is available free of charge at https://pubs.acs.org/doi/10.1021/acs.langmuir.4c00585.
Overnight deposition of MHC produces the largest gain (Figure S1); packing densities of vancomycin-, tryptophan-, and phenylalanine-detecting EAB sensors fabricated using 500 nM aptamer and 1, 10, 100, or 1000 μM MCH (Figure S2); all three of our test-bed sensors exhibit acceptably large SWV peak currents (Figure S3); packing densities of vancomycin-, tryptophan-, and phenylalanine-detecting EAB sensors fabricated using 10 μM MCH and 100, 200, 500, or 1000 nM aptamer (Figure S4); sensors prepared in an “undiluted” mixture of 2 μM aptamer and 40 μM MCH and in a 10-fold dilution of this mixture (Figure S5); CD signal peaks of phenylalanine, vancomycin, and tryptophan aptamers (Figure S6); drift of vancomycin-, tryptophan-, and phenylalanine-detecting EAB sensors (Figure S7); and codeposition and sequential deposition both support accurate drift correction (Figure S8) (PDF)

Complete contact information is available at: https://pubs.acs.org/10.1021/acs.langmuir.4c00585

The authors declare no competing financial interest.

gain (relative change in signal upon the addition of high concentrations of the target) of the vancomycin and tryptophan sensors without significantly reducing their stability. In contrast, the gain of the phenylalanine sensor is effectively identical irrespective of the fabrication approach employed. This sensor, however, appears to employ binding-induced displacement of the redox reporter rather than binding-induced folding as its signal transduction mechanism, suggesting in turn a mechanism for the improvement observed for the other two sensors. Codeposition thus not only provides a more convenient means of fabricating EAB sensors but also can improve their performance.

Graphical Abstract

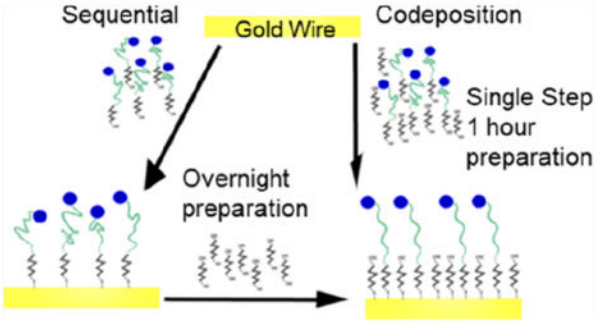

INTRODUCTION

Electrochemical aptamer-based (EAB) sensors support the high-frequency, real-time measurement of specific molecules irrespective of their chemical or enzymatic reactivity, rendering the approach general. EAB sensors are also selective enough that they can perform such measurements even when challenged in complex sample matrices, such as undiluted saliva,[1] foodstuffs,[2] urine,[3] serum,[4] and whole blood.[5] Indeed, the approach even supports real-time, high-temporal-resolution molecular monitoring in situ in the living body,[6–12] an ability that, in turn, supports closed-loop, feedback controlled drug delivery.[6,10,13]

EAB sensors comprise a redox-reporter-modified, electrode-bound aptamer that undergoes a conformational change upon target binding (Figure 1). This, in turn, changes the rate of electron transfer to the electrode, generating an electrochemical signal directly reflecting the target concentration (Figure 1). A critical step in the fabrication of EAB sensors is attachment of the target-recognizing aptamer to the interrogating electrode, which is achieved using a thiol-on-gold self-assembled monolayer (SAM). Historically, this has been performed by sequentially soaking the gold surface in a solution of a thiol-modified aptamer followed by a second incubation in dilute mercaptohexanol (MCH), which serves to “backfill” the space between aptamers to form a continuous monolayer (Figure 1). Since it was first reported for the fabrication of DNA-modified SAMS,[14–16] this “sequential” method has dominated prior reports of EAB sensor fabrication, which typically employed MCH deposition times ranging from a few hours to overnight.[4,6,11,17–19] In contrast to this sequential method, however, there have also been reports in which other, similarly DNA-decorated gold surfaces (e.g., refs 20–24) and, more recently, even EAB sensors[25,26] have been fabricated via a “codeposition” method that employs single-step incubation in

a mixture of MCH and thiol-modified aptamer (Figure 1). To date, however, we have not seen any comparison of the performance of EAB sensors fabricated using these two distinct approaches. Performing such a comparison here, we find that, in addition to being somewhat more convenient, codeposition can also improve EAB sensor performance.

RESULTS AND DISCUSSION

Here we compare the performance of EAB sensors fabricated using either the more commonly employed "sequential deposition," in which incubation in aptamer is followed by incubation in an MCH solution, or "codeposition," in which the electrode is incubated in a mixture of aptamer and MCH. Of note, although overnight incubation in MCH is commonly employed in the sequential deposition fabrication of EAB sensors,[4,6,13,18] some authors have used shorter periods.[17,19] We find, however, that longer incubation in MCH leads to improved performance for sensors fabricated using the sequential deposition method (Figure S1). Given this, we used overnight MCH incubation as the sequential deposition "standard" against which we performed our comparisons.

Codeposition improves the signal gain of some EAB sensors. To see this, we first employed an established vancomycin-detecting sensor.[6] When fabricated using the sequential method (500 nM aptamer for 1 h followed by 10 mM MCH overnight), the signal gain of these sensors is 91 ± 1% (Figure 2A; reported confidence intervals reflect the standard deviation across multiple, independently fabricated devices). In contrast, when we fabricated sensors via codeposition in a single solution containing the thiol-modified aptamer at 500 nM and MCH at 10 μM, the gain rises to 121 ± 4% (Figure 2A). The improvement in gain, however, depends on the concentration of MCH employed and falls significantly at both lower and higher MCH concentrations (Figure 2A). Building on these results, we find similarly improved gain when we use codeposition to fabricate a tryptophan-detecting sensor,[27] with the highest gain seen at 10 μM MCH and lower gain at concentrations above or below this (Figure 2B). For a phenylalanine-detecting sensor,[28] in contrast, the highest gain we obtained via codeposition only equaled, rather than surpassed, that produced by the sequential method (Figure 2C).

The poorer gain seen at lower and higher MCH concentrations appears to arise as a result of poor monolayer formation and small peak currents under the former and latter conditions, respectively. Specifically, we observe upward sloping baselines at negative potentials for sensors fabricated using codeposition at 1 μM MCH (Figure 2D–F), an effect that is indicative of oxygen reduction occurring because of a poorly formed monolayer.[29] Besides, faradaic processes, such as nonspecific adsorption of the DNA probes on gold surface and hydrogen reduction, may also attribute to the low signal gain at lower MCH concentration.[30] Sensors fabricated by using codeposition at high MCH concentrations, in contrast, produce only weak methylene blue peaks (Figure 2D–F). This presumably occurs because too few aptamers are immobilized on the electrode under these conditions. Consistent with the latter argument, when we determined the packing density (number of aptamers per unit area) for all three sensors, we found that the packing density falls by about 2 orders of magnitude as the MCH concentration rises from 10 μM to 1 mM (Figure S2).

The gain of sensors fabricated via codeposition is a weaker function of aptamer concentration than of the MCH concentration. Specifically, when we hold the MCH concentration fixed at 10 μM, the titration curves of the resulting sensors are effectively unchanged using aptamer deposition concentrations varying from 100 nM to 1 μM (Figure 3A–C), and all of the resulting sensors exhibit reasonable peak currents when interrogated using square wave voltammetry (Figure S3). Likewise, the packing densities for all such sensors are, at around 10^{-13} mol/cm^2, closely comparable (Figure S4). We note, however, that because of low methylene blue peak currents at lower aptamer concentrations and the prohibitive cost of employing higher aptamer concentrations, the range of DNA concentrations that can be employed in EAB sensor fabrication is much smaller than the range of MCH concentrations we explored in the prior paragraph.

A number of previous reports have emphasized the need to optimize the aptamer/MCH ratio used in sensor fabrication.[22,23,31] Perhaps not surprisingly, however, this result does not hold at arbitrarily low concentrations of the two. Specifically, when we characterized sensors prepared via codeposition at a fixed 1:20 aptamer/MCH ratio and aptamer concentrations ranging from 2 μM aptamer down to 2 nM, we find that, consistent with prior claims, sensor performance does not vary significantly over the range of concentrations that still ensure measurable sensor performance. That is, at aptamer and MCH concentrations below 200 nM and 4 μM MCH, respectively, the methylene blue peak is lost, suggesting that little DNA has adsorbed to the electrode, and the baselines slope strongly upward, suggesting a poorly formed monolayer (Figure S5A).

Previously, Xiao and co-workers have shown that EAB sensor gain can be increased by performing aptamer deposition in the presence of its target.[32] In keeping with this, when we employ sequential deposition, the signal gain of our vancomycin-detecting sensor improves from the 96.6 ± 0.2% in the absence of a target to 102.6 ± 1.4% with target-assisted sequential deposition (Figure 4A). Moreover, this improvement is additive with the improvements associated with codeposition. That is, the gain of our vancomycin-detecting sensor rises from 118.3 ± 2.1% for codeposition in the absence of a target to 146.7 ± 0.6% when we perform codeposition at 1 mM target. The gain of our tryptophan-detecting sensor is enhanced still more significantly, rising from 210.0 ± 4.8% for codeposition in the absence of a target to 368.2 ± 8.0% (Figure 4B). In contrast, however, either alone or in combination, codeposition and target-assisted deposition did not significantly improve the gain of the phenylalanine-detecting sensor (Figure 4C).

We suspect that the lack of improvement seen for the phenylalanine sensor with either codeposition or target-assisted deposition occurs because, in contrast to the aptamers employed in our other two sensors, the phenylalanine aptamer remains folded in the absence of a target. For example, whereas both the vancomycin and tryptophan aptamers exhibit significant changes in their circular dichroism spectrum upon target binding, suggesting that they undergo binding-induced folding, the phenylalanine aptamer does not (Figure 5). Upon addition of the denaturant urea, the ellipticity of the phenylalanine aptamer also falls much more significantly than that of the other aptamers (Figure S6), again suggesting that, unlike the other aptamers we have employed, it is folded in the absence of a target. Presumably, this means that the binding-induced signal change associated

with the phenylalanine sensor is likely generated by target-induced displacement of the redox reporter from the target binding pocket.[33] That this aptamer is always folded may account for the inability of codeposition and target-assisted deposition to improve its gain. Specifically, unfolded aptamers expose their nucleobases, which are then free to bind the surface of our gold electrodes nonspecifically.[34] Such nonspecific adsorption would produce a background of methylene blue peak current that does not respond to the target, reducing gain. Codeposition and target-assisted deposition may reduce this by limiting opportunities for the solvent-exposed bases in unfolded molecules to interact with the gold, in the latter case by reducing the concentration of unfolded molecules.

The stability of sensors fabricated via codeposition matches that seen for sensors fabricated via sequential deposition. To see this, we exposed sensors to 37 °C whole blood, conditions we employ to mimic in vivo sensor placements.[35] Under these conditions, the signals from all three sensors rapidly fall at all square-wave frequencies (Figure S7). To correct this drift, we typically interrogate in vivo EAB sensors at a pair of square-wave frequencies that drift in concert, and use these to perform kinetic differential measurements, a drift correction approach.[12] For our vancomycin- and tryptophan-detecting sensors, we find that the accuracy of this drift correction (in 37 °C whole blood in vitro) is effectively identical for devices fabricated using either codeposition or sequential deposition (Figure S8A,B). For our phenylalanine-detecting sensor, however, we find that devices fabricated using codeposition exhibit a slightly higher residual drift after KDM correction (Figure S8C).

The performance of sensors fabricated by using codeposition is largely independent of deposition time. Specifically, the gain and binding midpoints of sensors fabricated using a 1 h deposition time are indistinguishable from those of sensors fabricated using longer deposition times (Figure 6A–C). The drift seen in undiluted 37 °C whole blood is similarly independent of the deposition time (Figure 6D–F). Such single-step, 1 h deposition is faster and more convenient than the overnight incubations we have generally employed for sequential deposition. And, as we note above, although sequential deposition can be performed more rapidly, this harms sensor performance (Figure S1).

CONCLUSIONS

Codeposition improves the gain of some EAB sensors and, when combined with target-assisted deposition, generates some of the highest gain sensors we have achieved to date. Circular dichroism studies suggest that the aptamers that codeposition improves are those that employ binding-induced folding as their signal transduction mechanism; the approach has little impact on the performance of our phenylalanine sensor, which appears to instead employ binding-induced displacement of the redox reporter as its signal transduction mechanism. For all aptamers, codeposition is more rapid, being a single-step deposition process that requires only 1 h, a time scale far faster than the overnight incubations required to achieve the best performance by using sequential deposition. In short, codeposition is a more convenient means of fabricating EAB sensors that achieves better or at least comparable performance to the more commonly employed sequential deposition method.

METHODS AND MATERIALS

Materials.

Phosphate-buffered saline (PBS) and salts were obtained from Santa Cruz Biotechnology (Dallas, TX), cow blood was from Hemostat Laboratory (Dixon, CA), phenylalanine was from Sigma-Aldrich (Saint Louis, MO), and vancomycin and tryptophan were from Thermal Fisher Scientific (Waltham, MA). Gold wires (75 μm diameter, 64 μm insulation thickness) were purchased from A-M Systems (Sequim, WA), and PTFE tubing (HS Sub-Lite-Wall, 0.02 in., black opaque) was from Zeus (Branchburg Township, CA). The 60/40 lead–selenium solder was purchased from Digikey (Thief River Falls, MN). Platinum counter electrodes, Ag/AgCl (3 M KCl) reference electrodes, and gold-plated pin connectors were obtained from CH Instruments (Austin, TX). The PBS used in our experiments contains 2 mM $MgCl_2$ to mimic the concentration of this divalent cation found in blood.

We obtained the relevant thiol- and methylene-blue-modified aptamers and corresponding oligonucleotides from IDT (Newark, NJ) and used these as received. We employed three aptamer sequences (Table 1), each with the following structure:

$$5' - HO - (CH_2)_6 - S - S - (CH_2)_6 - O - PO_2O - \text{aptamer sequence} - O - CH_2 - CH(CH_2OH) - NH - C(O) - (CH_2)_2 - MB - 3'$$

Electrode Preparation.

We fabricated the EAB sensor electrodes as follows. Briefly, we cut 4.5 cm segments of gold wire, soldered one of its ends to a gold-plated pin connector with 60/40 lead–selenium solder, and insulated the gold wire with heat-shrinkable PTFE tubing, leaving approximately 3 mm wire exposed as the working electrode. We then cleaned the gold surface using established protocols.[16,36] In these, we first exposed the bare gold wire to 0.5 M NaOH and performed electrochemical cleaning (using external reference and counter electrodes and a CHI 1040C Electrochemical Workstation from CH Instruments, Austin, TX) by cycling the potential 300 times between −1 and −1.6 V (all potentials vs Ag/AgCl) at 1 V/s to remove any residual contaminants on the electrode surface. Following this, we rinsed the electrode and performed pulsing between 0 and 2 V for 16,000 cycles with a pulse length of 0.02 s in 0.5 M H_2SO_4 to increase the microscopic surface area of the electrodes.[16] We then immersed the electrodes in 0.5 M H_2SO_4 and cycled the potential two times between 1.50 and −0.35 V at 100 mV/s. Finally, we rinsed the freshly cleaned electrodes with a deionized water.

Deposition Procedures.

We prepared a 1-mercaptohexanol (MCH) solution and reduced DNA solution for sequential deposition or mixed solution of MCH and reduced DNA for codeposition. The manufacturer provides the DNA constructs in a disulfide form, which we reduced before deposition by combining 6 μL of 10 mM Tris(2-carboxyethyl)phosphine (TCEP) per microliter of the DNA-aptamer at 100 μM and incubating for 1 h in the dark at room temperature. We prepared 10 mM MCH by dissolving 4.05 μL of pure MCH in 3 mL of PBS and then diluted

this with PBS to the desired final concentration. For our studies of MCH concentration dependence, we combined the appropriate concentration MCH solution with 3.5 μL of reduced DNA solution and 86.5 μL of PBS to obtain 100 μL of solution of 500 μM DNA with the appropriate concentration of MCH. For our studies of the DNA concentration dependence, we combined 10 μL of 100 μM MCH with 7, 3.5, 1.4, or 0.7 μL reduced DNA solution and then diluted them to 100 μL in PBS. For sequential deposition, we prepared sensors by immersing clean electrodes in 200 nM reduced DNA solution for 1 h and then in 10 mM MCH solution overnight or for several hours as stated in the caption. For codeposition, we prepared sensors by immersing clean electrodes in the appropriate DNA/MCH solution either overnight or for shorter periods as indicated. We rinsed all of the sensors with deionized water prior to measurements.

Measurement and Data Processing.

We interrogated all EAB sensors using square-wave voltammetry (SWV) on a CHI 1040C Electrochemical Workstation over the potential range −0.20 to −0.45 V (all potentials relative to Ag/AgCl) and an amplitude of 25 mV. We used a standard three-electrode set up employing a platinum counter electrode and a Ag/AgCl (3 M KCl) reference electrode.[37]

For the experiments we conducted in PBS, we performed measurements at 37 °C and after at least 3 min equilibration to ensure that the proper temperature had been achieved. To produce binding curves (Figures 2A–C, 3A–C, 4A–C, and 6A–C), we extracted the voltametric peak current at each target concentration. We converted these into “normalized signal changes” by determining the percentage difference between the peak current seen at a given target concentration and the corresponding peak height measured in a PBS blank:

$$\text{Normalized signal}(\%) = \frac{I_{\text{target}} - I_{\text{blank}}}{I_{\text{blank}}} \times 100\% \tag{1}$$

Kinetic differential measurements (KDMs) were calculated by taking the difference between the normalized signal seen at the lower frequency and that seen at the higher frequency:

$$\text{KDM}(\%) = \frac{\text{normalizedsignal}_{\text{frequency}} - \text{normalizedsignal}_{\text{low frequency}}}{1 + \frac{\text{normalizedsignal}_{\text{high frequency}} + \text{normalizedsignal}_{\text{low frequency}}}{2}} \times 100\% \tag{2}$$

For phenylalanine, the frequencies we employed were 25 and 300 Hz; for tryptophan, they were 15 and 200 Hz; and for vancomycin, they were 20 and 200 Hz. For vancomycin constructs, we fit these data sets to the Langmuir isotherm to determine their signal gain (ΔS):

$$S(T) = \frac{[T]\Delta S}{[T] + K_{\text{D}}} \tag{3}$$

where S(T) is the EAB sensor KDM signal seen in the presence of different concentrations of target, [T] is the target concentration, and K_D is its dissociation constant. For phenylalanine constructs, the titration curve does not reach saturation upper baseline because of the phenylalanine solubility limit. Thus, it cannot be properly fitted with this model, and we used the signal gain of phenylalanine-detecting sensor at 20 mM as the overall signal gain (ΔS).

Because the tryptophan aptamer nonequivalently binds two copies of its target,[27] we fit its binding data to the sum of two Langmuir isotherms:

$$S(T) = \frac{[T]\Delta S_1}{[T] + K_{D1}} + \frac{[T]\Delta S_2}{[T] + K_{D2}} \quad (4)$$

where S(T) is the EAB sensor KDM signal seen in the presence of different concentrations of target, [T] is the target concentration, ΔS_1 and ΔS_2 are the changes in signal associated with the two binding events, and K_{D1} and K_{D2} are their dissociation constants. For this sensor, we defined the gain as the sum of the ΔS_1 and ΔS_2.

For experiments performed in undiluted bovine blood, we interrogated the sensors continuously at 37 °C by using a temperature-controlled water bath. Under these conditions, EAB sensors exhibit an initial exponential drift followed by a linear drift.[35] We calculated the "normalized signal change" of each measurement by determining the percentage difference between the peak current seen at each measurement to the corresponding peak height measured at 90 min, which is during the linear drift phase.

$$\text{Normalized signal}(\%) = \frac{I_{\text{measurement}} - I_{90\ \text{min}}}{I_{90\ \text{min}}} \times 100\% \quad (5)$$

We performed kinetic differential measurements (KDMs) between the normalized signal seen at 30 and 100 Hz (eq 2) and plotted the signal change over time.

For probe packing density measurements, chronocoulometric experiments were acquired using PBS rather than 0.5 mM RuHex in 10 mM Tris buffer. Electrodes were immersed in the respective solution for 10 min prior to the experiment. Two-step coulometry was performed stepping from 0 to −0.350 to 0 V with a pulse period of 250 ms. The probe densities were calculated by using a previously established method.

Circular Dichroism Spectroscopy.

We monitored the ureainduced unfolding and target-binding conformational change of the three aptamers as follows. We made solutions of 1 μM aptamer and the appropriate urea concentration in PBS at pH 7.4 and allowed them equilibrate for at least 3 min at 20 °C before then measuring their CD spectra on a J-1500 Circular Dichroism Spectrophotometer (Jasco Products Company, Oklahoma City, OK) using a 1 cm path length cuvette. We

then measured the CD signals of the three aptamers in the presence and absence of their target. For these experiments, we recorded the CD spectra of 1 μM aptamer solutions lacking the target; 1 μM aptamer solutions containing 40 μM target (phenylalanine), 50 μM target (tryptophan), or 1 mM target (vancomycin); and solutions of the target at these same concentrations but lacking aptamer. As phenylalanine and vancomycin target-only solution produced large CD signals, we subtracted the CD signal of 1 μM aptamer solution containing target by that of only target solution to get the CD signal of aptamer bound with corresponding target.

Supplementary Material

Refer to Web version on PubMed Central for supplementary material.

REFERENCES

(1). Baker BR; Lai RY; Wood MS; Doctor EH; Heeger AJ; Plaxco KW An electronic aptamer-based small-molecule sensor for the rapid, label-free detection of cocaine in adulterated samples and biological fluids. J. Am. Chem. Soc 2006, 128, 3138–3139. [PubMed: 16522082]

(2). Li H; Somerson J; Xia F; Plaxco KW Electrochemical DNA-based sensors for molecular quality control: Continuous, real-time melamine detection in flowing whole milk. Anal. Chem 2018, 90, 10641–10645. [PubMed: 30141321]

(3). Idili A; Arroyo-Currás N; Ploense KL; Csordas A; Kuwahara M; Kippin TE; Plaxco KW Seconds-resolved pharmacokinetic measurements of the chemotherapeutic irinotecan in situ in the living body. Chem. Sci 2019, 10, 8164–8170. [PubMed: 31673321]

(4). Lai RY; Plaxco KW; Heeger AJ Aptamer-based electrochemical detection of picomolar platelet-derived growth factor directly in blood serum. Anal. Chem 2007, 79, 229–233. [PubMed: 17194144]

(5). Downs AM; Gerson J; Leung KK; Honeywell KM; Kippin T; Plaxco KW Improved calibration of electrochemical aptamer-based sensors. Sci. Rep 2022, 12, 5535. [PubMed: 35365672]

(6). Dauphin-Ducharme P; Yang K; Arroyo-Currás N; Ploense KL; Zhang Y; Gerson J; Kurnik M; Kippin TE; Stojanovic MN; Plaxco KW Electrochemical aptamer-based sensors for improved therapeutic drug monitoring and high-precision, feedback-controlled drug delivery. ACS Sensors 2019, 4, 2832–2837. [PubMed: 31556293]

(7). Wu Y; Tehrani F; Teymourian H; Mack J; Shaver A; Reynoso M; Kavner J; Huang N; Furmidge A; Duvvuri A; Nie Y; Laffel LM; Doyle FJ 3rd; Patti ME; Dassau E; Wang J; Arroyo-Currás N Microneedle Aptamer-Based Sensors for Continuous, Real-Time Therapeutic Drug Monitoring. Anal. Chem 2022, 94, 8335–8345. [PubMed: 35653647]

(8). Lin S; Cheng X; Zhu J; Wang B; Jelinek D; Zhao Y; Wu TY; Horrillo A; Tan J; Yeung J; Yan W; Forman S; Coller HA; Milla C; Emaminejad S Wearable microneedle-based electrochemical aptamer biosensing for precision dosing of drugs with narrow therapeutic windows. Sci. Adv 2022, 8, No. eabq4539. [PubMed: 36149955]

(9). Chamorro-Garcia A; Gerson J; Flattebo C; Fetter L; Downs AM; Emmons N; Ennis HL; Milosavic N; Yang K; Stojanovic M; Ricci F; Kippin TE; Plaxco KW Real-time, seconds-resolved measurements of plasma methotrexate in situ in the living body. ACS Sens. 2023, 8, 150–157. [PubMed: 36534756]

(10). Gerson J; Erdal MK; McDonough MH; Ploense KL; Dauphin-Ducharme P; Honeywell KM; Leung KK; ArroyoCurras N; Gibson JM; Emmons NA; Meiring W; Hespanha JP; Plaxco KW; Kippin TE High-precision monitoring of and feedback control over drug concentrations in the brains of freelymoving rats. Sci. Adv 2023, 9, No. eadg3254. [PubMed: 37196087]

(11). Arroyo-Currás N; Scida K; Ploense KL; Kippin TE; Plaxco KW High surface area electrodes generated via electrochemical roughening improve the signaling of electrochemical aptamer-based biosensors. Anal. Chem 2017, 89, 12185–12191. [PubMed: 29076341]

(12). Arroyo-Currás N; Somerson J; Vieira P; Ploense K; Kippin TE; Plaxco KW Real-time measurement of small molecules in awake, ambulatory animals. Proc. Natl. Acad. Sci. U. S. A 2017, 114, 645–650. [PubMed: 28069939]

(13). Arroyo-Currás N; Ortega G; Copp DA; Ploense KL; Plaxco ZA; Kippin TE; Hespanha JP; Plaxco KW HighPrecision Control of Plasma Drug Levels Using Feedback-Controlled Dosing. ACS pharmacology & translational science 2018, 1 (2), 110–118. [PubMed: 32219207]

(14). Herne TM; Tarlov MJ Characterization of DNA probes immobilized on gold surfaces. J. Am. Chem. Soc 1997, 119, 8916–8920.

(15). Levicky R; Herne TM; Tarlov MJ; Satija SK Using selfassembly to control the structure of DNA monolayers on gold: A neutron reflectivity study. J. Am. Chem. Soc 1998, 120, 9787–9792.

(16). Mandler D; Kraus-Ophir S Self-assembled monolayers (SAMs) for electrochemical sensing. J. Solid State Electrochem 2011, 15, 1535.

(17). Xie Y; Wu S; Chen Z; Jiang J; Sun J Rapid nanomolar detection of methamphetamine in biofluids via a reagentless electrochemical aptamer-based biosensor. Analytica chimica acta 2022, 1207, No. 339742. [PubMed: 35491035]

(18). Li S; Ferrer-Ruiz A; Dai J; Ramos-Soriano J; Du X; Zhu M; Zhang W; Wang Y; Herranz MÁ; Jing L; Zhang Z; Li H; Xia F; Martín N A pH-independent electrochemical aptamer-based biosensor supports quantitative, real-time measurement in vivo. Chem. Sci 2022, 13, 8813–8820. [PubMed: 35975161]

(19). Yuan Y; Bali A; White RJ; Heikenfeld J Solution-Phase Electrochemical Aptamer-Based Sensors. IEEE transactions on bio-medical engineering 2023, 70, 824–830. [PubMed: 36063526]

(20). Sauthier ML; Carroll RL; Gorman CB; Franzen S Nanoparticle Layers Assembled through DNA Hybridization: Characterization and Optimization. Langmuir 2002, 18, 1825–1830.

(21). Steichen M; Buess-Herman C Electrochemical detection of the immobilization and hybridization of unlabeled linear and hairpin DNA on gold. Electrochem. 2005, 7, 416–420.

(22). Keighley SD; Li P; Estrela P; Migliorato P Optimization of DNA immobilization on gold electrodes for label-free detection by electrochemical impedance spectroscopy. Biosens Bioelectron. 2008, 23, 1291–1297. [PubMed: 18178423]

(23). Henry OY; Perez JG; Sanchez JL; O'Sullivan CK Electrochemcial characterisation and hybridisation efficiency of coassembled monolayers of PEGylated ssDNA and mercaptohexanol on planar gold electrodes. Biosens Bioelectron. 2010, 25, 978–983. [PubMed: 19800782]

(24). Ferrario A; Scaramuzza M; Pasqualotto E; De Toni A; Paccagnella A Coadsorption optimization of DNA in binary self-assembled monolayer on gold electrode for electrochemical detection of oligonucleotide sequences. JEAC 2013, 689, 57–62.

(25). Shaver A; Curtis SD; Arroyo-Currás N Alkanethiol monolayer end groups affect the long-term operational stability and signaling of electrochemical aptamer-based sensors in biological fluids. ACS Appl. Mater. Interface 2020, 12, 11214–11223.

(26). Shaver A; Kundu N; Young BE; Vieira PA; Sczepanski JT; Arroyo-Currás N Nuclease hydrolysis does not drive the rapid signaling decay of DNA aptamer-based electrochemical sensors in biological fluids. Langmuir 2021, 37, 5213–5221. [PubMed: 33876937]

(27). Wu Y; Ranallo S; Del Grosso E; Chamoro-Garcia A; Ennis HL; Milosavić N; Yang K; Kippin T; Ricci F; Stojanovic M; Plaxco KW Using spectroscopy to guide the adaptation of aptamers into electrochemical aptamer-based sensors. Bioconj. Chem 2023, 34, 124–132.

(28). Cheung KM; Yang KA; Nakatsuka N; Zhao C; Ye M; Jung ME; Yang H; Weiss PS; Stojanović MN; Andrews AM Phenylalanine monitoring via aptamer-field-effect transistor sensors. ACS Sensors 2019, 4, 3308–3317. [PubMed: 31631652]

(29). Ehlich J; Migliaccio L; Sahalianov I; Nikić M; Brodský J; Gablech I; Vu XT; Ingebrandt S; Głowacki ED Direct measurement of oxygen reduction reactions at neurostimulation electrodes. J. Neural Eng 2022, 19, No. 036045.

(30). Lichtenberg JY; Ling Y; Kim S Non-Specific Adsorption Reduction Methods in Biosensing. Sensors (Basel). 2019, 19, 2488. [PubMed: 31159167]

(31). Zhang X; Yadavalli VK Surface immobilization of DNA aptamers for biosensing and protein interaction analysis. Biosens. Bioelectron 2011, 26, 3142–3147. [PubMed: 21227676]

(32). Liu Y; Canoura J; Alkhamis O; Xiao Y Immobilization strategies for enhancing sensitivity of electrochemical aptamer-based sensors. ACS Appl. Mater. Interfaces 2021, 13, 9491–9499. [PubMed: 33448791]

(33). Dauphin-Ducharme P; Churcher ZR; Shoara AA; Rahbarimehr E; Slavkovic S; Fontaine N; Boisvert O; Johnson PE Redox Reporter - Ligand Competition to Support Signaling in the Cocaine-Binding Electrochemical Aptamer-Based Biosensor. Chemistry - Eur. J 2023, 29, No. e202300618.

(34). Kimura-Suda H; Petrovykh DY; Tarlov MJ; Whitman LJ Base-dependent competitive adsorption of single-stranded DNA on gold. J. Am. Chem. Soc 2003, 125, 9014–9015. [PubMed: 15369348]

(35). Leung KK; Downs AM; Ortega G; Kurnik M; Plaxco KW Elucidating the mechanisms underlying the signal drift of electrochemical aptamer-based Sensors in whole blood. ACS Sensors 2021, 6, 3340–3347. [PubMed: 34491055]

(36). Idili A; Gerson J; Parolo C; Kippin TE; Plaxco KW An electrochemical aptamer-based sensor for the rapid and convenient measurement of L-tryptophan. Anal. Bioanal. Chem 2019, 411, 4629–4635. [PubMed: 30796485]

(37). Lao R; Song S; Wu H; Wang L; Zhang Z; He L; Fan C Electrochemical Interrogation of DNA Monolayers on Gold Surfaces. Anal. Chem 2005, 77, 6475–6480. [PubMed: 16194115]

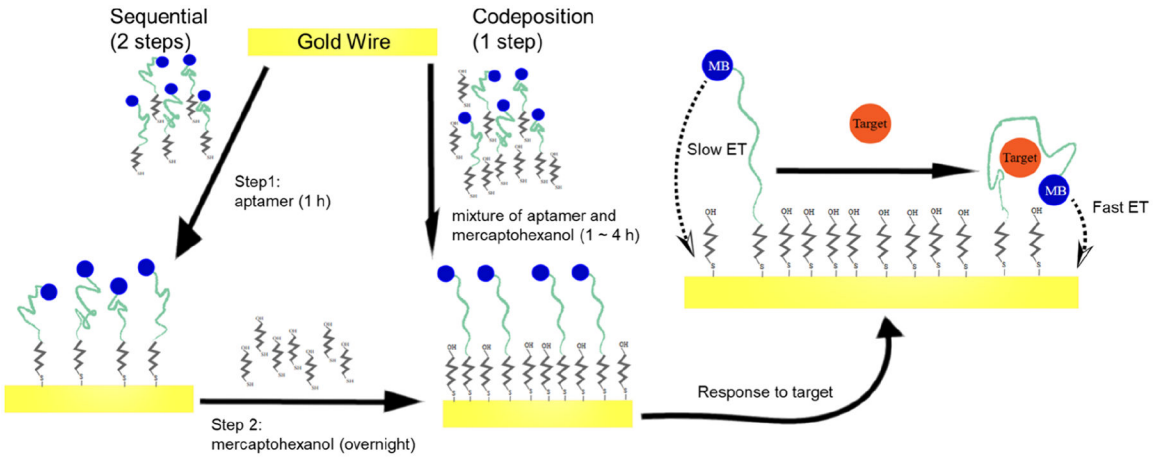

Figure 1.

EAB sensors have most often been fabricated using a “sequential deposition” in which a gold electrode is exposed to a solution of thiol-modified aptamer followed by an overnight “backfilling” incubation in dilute mercaptohexanol (MCH). Here we compare the advantages of this approach via a “codeposition” approach in which only a mixed solution of mercaptohexanol and a thiol-modified aptamer is employed. Although the latter has seen widespread use in the fabrication of DNA-modified monolayers, it has rarely been employed in the fabrication of sensors of this specific type.

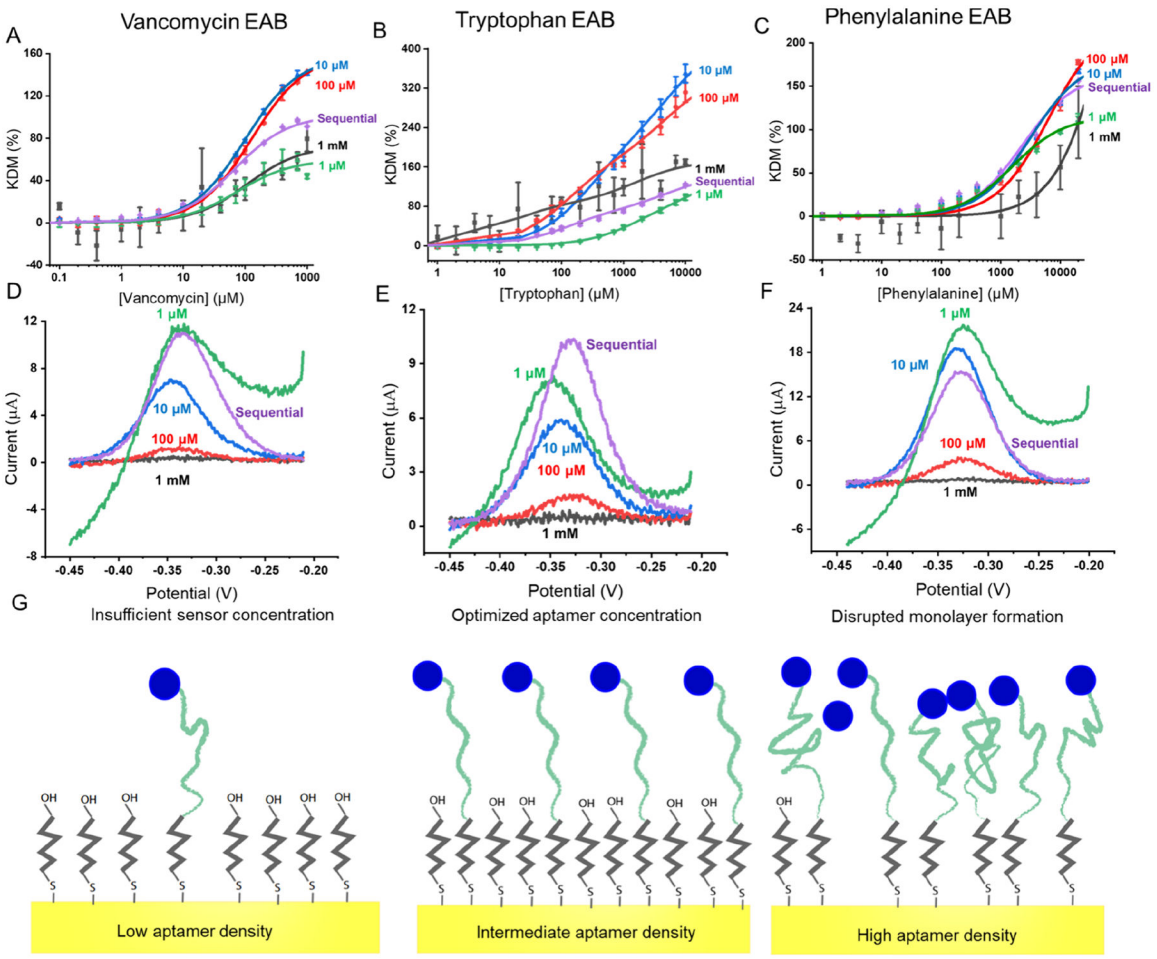

Figure 2.

Codeposition often improves EAB sensor gain, which is the relative signal change from no target to high target concentrations. (Top row) Shown are binding curves for (A) vancomycin-, (B) tryptophan-, and (C) phenylalanine-detecting EAB sensors when the sensors are fabricated using sequential deposition (500 nM aptamer followed by 10 mM MCH) or codeposition (500 nM aptamer at the indicated MCH concentration). In each case, codeposition at 10 or 100 μM MCH gives rise to gain that matches or improves on the gain seen for sensors fabricated using sequential deposition. In contrast, at higher or lower MCH concentrations, the gains were obtained using codeposition fall. (D, E, F) The poorer gain seen at lower MCH concentrations is associated with voltammogram baselines that slant strongly upward, suggesting that oxygen reduction is occurring as a result of incomplete monolayer formation (illustrated in panel G). In contrast, the methylene blue peak is suppressed upon codeposition at higher MCH, presumably because fewer aptamers are immobilized under these conditions. Only at intermediate MCH concentrations are these problems avoided to create high-performance sensors. The data presented here were collected from sensors fabricated via overnight deposition for codeposition and 1 h aptamer deposition followed by overnight MCH deposition for sequential deposition.

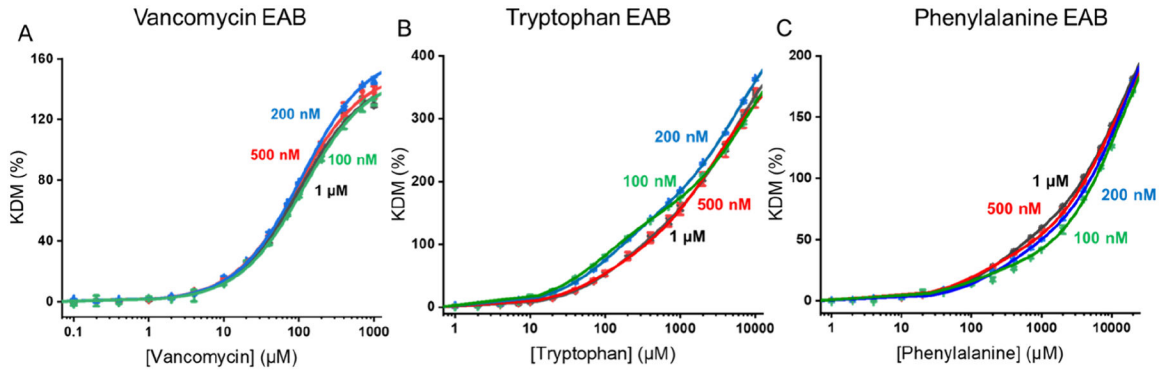

Figure 3.

(A–C) The signaling properties of sensors fabricated via codeposition are only a weak function of the concentration of DNA employed during deposition. Here we employed overnight codeposition.

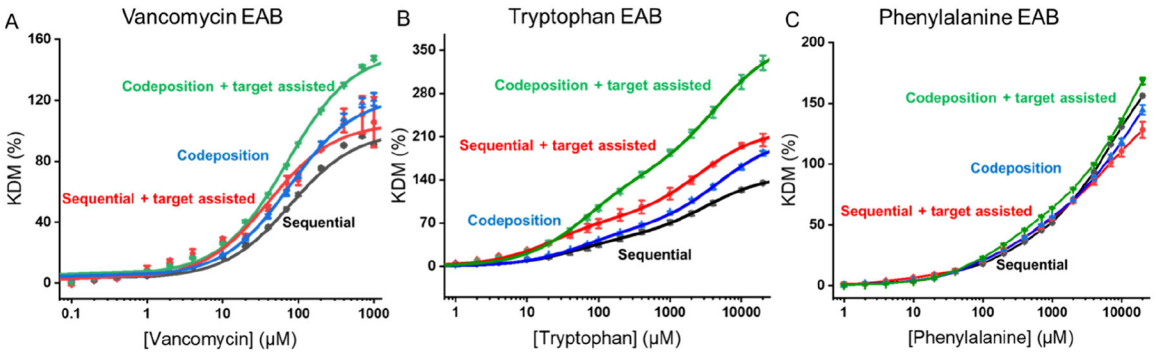

Figure 4.

Signal gains (e.g., where the fitted Langmuir isotherms hit the right side of these plots) of our (A) vancomycin- and (B) tryptophan-detecting EAB sensors increase when they are fabricated in the presence of their target. This effect occurs for both sequential and codeposition and is additive with the improvements obtained via codeposition. (C) In contrast, the gain of our phenylalanine-detecting sensor varies little across these fabrication methods. The data presented here reflect sensors fabricated using overnight deposition for both codeposition and sequential deposition (i.e., in the MCH backfill solution overnight). We used overnight sequential deposition as the performance of sensors fabricated using this longer deposition time is improved relative to sensors fabricated using shorter incubations (Figure S1).

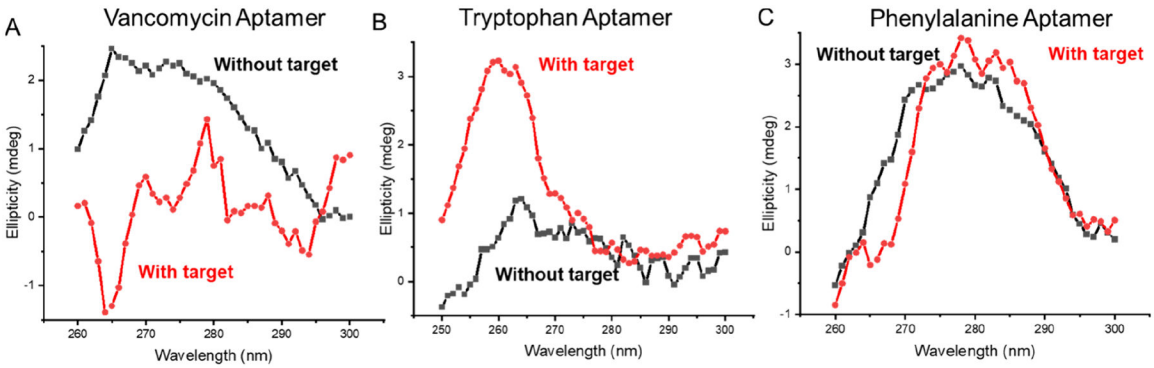

Figure 5.

Circular dichroism spectra of the vancomycin-binding and tryptophan-binding aptamers change dramatically between their target-bound and unbound statues (A, B), suggesting that target binding induces a large conformation change. (C) In contrast, the phenylalanine-binding aptamer shows no such change, suggesting that it remains folded even in the absence of a target.

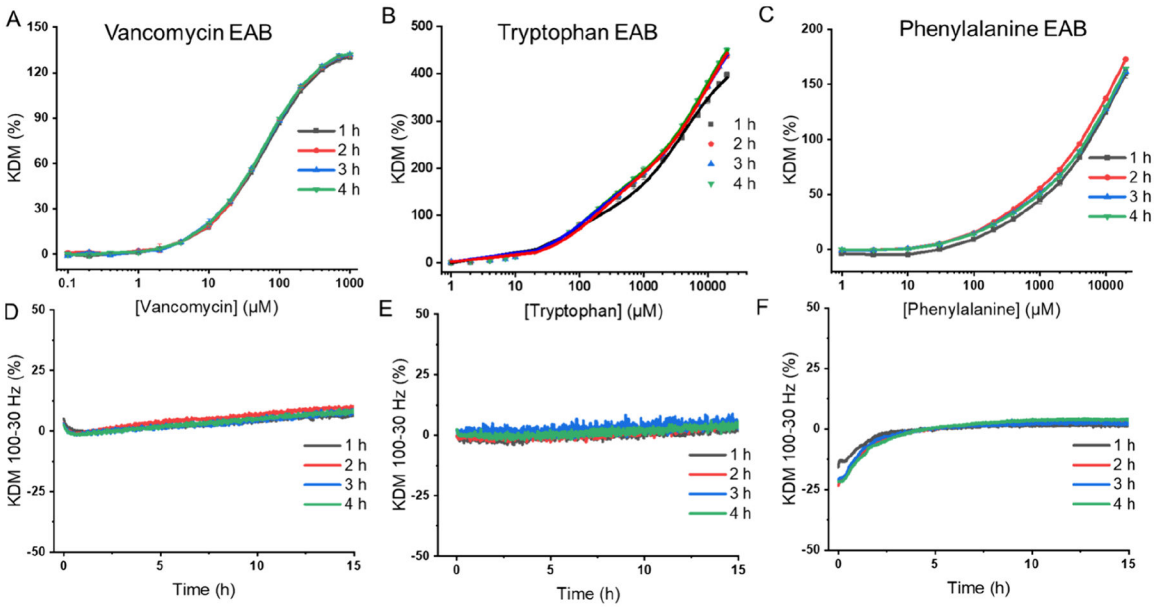

Figure 6.

Signaling and drift properties of EAB sensors are independent of the duration of the codeposition (deposition times indicated). Indicated in each panel are the codeposition times we employed.

Table 1.

Aptamer Sequences Used

	composition ($5' \rightarrow 3'$)
vancomycin	CGA GGG TAC CGC AAT AGT ACT TAT TGT TCG CCT ATT GTG GGT CGG
tryptophan	CCG GTG GTG TAG TTC CGG CGT GGG GAA GG
phenylalanine	CGA CCG CGT TTC TTC CCA AGA AAG CAA GTA TTG GTT GGT CG